High-throughput in vitro drug screening and in vivo studies identify fenretinide as a brain-penetrant DMG therapeutic

Dannielle H. Upton[1,2], Jie Liu[1], Sandra M. George[1], Santosh Valvi[1], Caitlin Ung[1], Benjamin S. Rayner[1,2], Anjana Gopalakrishnan[1], Ruby Pandher[1,2], Aaminah Khan[1,2], Pooja Venkat[1], Chelsea Mayoh[1,2], Holly Holliday[1,2], Nicole Yeung[1], Hieu Nguyen[1], Laura Franshaw[1], Anahid Ehteda[1], Han Shen[1], Giovanna Farruggia[3], Isabella Orienti[3], C Patrick Reynolds[4], Maria Tsoli[1,2,†], David S. Ziegler[1,2,5, †*]

[1]Children's Cancer Institute, Lowy Cancer Research Centre, University of New South Wales, Sydney, NSW, Australia

[2]School of Clinical Medicine, University of New South Wales, Sydney, NSW, Australia

[3]Alma Mater Studiorum University of Bologna, Department of Pharmacy and Biotechnology, Bologna, Italy

[4]Cancer Center, School of Medicine, Texas Tech University Health Sciences Center, Lubbock, TX, USA

[5]Kid's Cancer Centre, Sydney Children's Hospital, Randwick, NSW, Australia.

[†] Contributed equally.

*Corresponding author: Prof David Ziegler, Kids Cancer Centre, Sydney Children's Hospital, High St, Randwick NSW 2031, Telephone: +61-2-93821730, Email: d.ziegler@unsw.edu.au

ABSTRACT

Background: Diffuse midline glioma, characterised by H3K27 alteration (DMG), is the predominant high-grade glioma in children. It commonly originates in the brainstem, yet effective treatments for these patients remain elusive.

Methods: To identify novel therapies for DMG, we conducted high-throughput drug screens (HTS) using biologically active, clinically approved compounds against DMG neurospheres. Multiple primary DMG cultures were utilised in conjunction with in vitro cytotoxicity and clonogenic assays to validate the efficacy of top compounds. Molecularly diverse patient-derived and transgenic DMG orthotopic models were employed to assess therapeutic efficacy alongside pharmacokinetic and immunohistochemical analyses. Mechanistic studies, including RNA sequencing, western blotting, and flow cytometry, were conducted to elucidate the antitumour efficacy of the most promising compound, fenretinide, in DMG cells.

Results: Through HTS, six compounds were identified and validated for their potent cytotoxic activity. However, most of these compounds failed to improve survival in an orthotopic Diffuse Midline Glioma (DMG) model due to limited blood-brain barrier (BBB) penetration. In contrast, fenretinide exhibited effective BBB penetration, significantly enhancing the survival of tumour-bearing animals. Mechanistic studies revealed that fenretinide increased reactive oxygen species (ROS) generation and induced apoptosis by inhibiting PDGFR α. RNA-sequencing further elucidated that fenretinide upregulates the Unfolded Protein Response (UPR) and endoplasmic reticulum (ER) stress pathways while downregulating neurogenesis. The in vivo antitumour efficacy of two fenretinide formulations was demonstrated in PDGFR α -amplified and transgenic DMG models.

Conclusion: This comprehensive study has identified new DMG therapeutic vulnerabilities and highlights fenretinide as a brain-penetrant, anti-DMG agent.

Keywords: DMG, fenretinide, high-throughput screening, therapeutic, PDX

Key points:

- Identified and validated 6 compounds with potent cytotoxic activity through HTS.
- Highlighted the limited BBB penetration of most agents in DMG models, hampering their efficacy.
- Demonstrated significant survival enhancement in DMG models with fenretinide.

Importance of the Study: DMGs are the most aggressive of all childhood cancers. This study demonstrated that despite *in vitro* activity, most drugs fail *in vivo* due to inadequate BBB permeation. In contrast, fenretinide successfully penetrated the BBB, exhibiting significant anti-tumour activity by inhibiting multiple oncogenic pathways, including PDGFRα, with promise for clinical translation.

Main text:

INTRODUCTION

Diffuse midline glioma, H3K27 altered (DMG), is a malignant childhood brain tumour and the most common form of high-grade glioma affecting children [1]. DMG most commonly originates in the brainstem and is usually not amenable to surgical resection due to its location and diffuse infiltrative nature. Despite multiple clinical trials, radiotherapy remains the only available standard treatment, transiently improving neurological function and temporarily halting disease progression in up to 70% of patients. However, the prognosis of DMG remains dismal, with over 90% of children dying within 2 years of diagnosis, demonstrating the urgent need to identify better treatment options [2].

Molecularly, DMGs are characterised by K27M mutations in H3.3 or H3.1 (78%); TP53 mutations (77%) which are not targetable and inactivating mutations of ATRX [3-5]. Other alterations include ACVR1 activating mutations (in 20–32% of cases); gene amplifications in receptor tyrosine kinases (RTKs), such as platelet-derived growth factor receptor (PDGFR) [6,7] and mutations of the phosphatidylinositol-4,5-bisphosphate 3-kinase (PI3K) cascade [8] and loss of phosphatase and tensin (PTEN) homologue in up to 40% of cases [9]. Recent studies have also identified that most H3K27M mutant DMGs resemble oligodendroglial precursor cells, which exhibit higher proliferation and overexpression of PDGFRα independently of a genetic mutation or amplification, suggesting the potential for therapeutic intervention against PDGFRα [10]. Despite these targetable molecular aberrations, trials of specific inhibitors of PDGFRα, such as imatinib, dasatinib and ponatinib have not demonstrated clinical efficacy [11]. One potential reason for the failure of targeted

agents in DMG is the blood-brain barrier (BBB), which has been shown to remain intact and restrict the delivery of systemically administered therapies, leading to ineffective concentrations in the tumour [12]. Thus, despite the *in vitro* activity of PDGFR inhibitors against DMG, most clinical trials have shown no survival benefit, likely due to their poor brain penetration [13,14].

Drug repurposing of already clinically approved therapeutics can overcome the lengthy and expensive process of developing targeted therapies [15]. High-throughput screening (HTS), an efficient method of screening large numbers of drug candidates, can determine the activity of clinically approved and available pharmacological compounds against tumour samples [15]. For example, HTS in cell lines derived from genetically engineered DMG mouse models using the RCAS/tv-a system identified BMS-754807 as a potential therapeutic agent [16]. Similarly, a targeted screen of 83 drugs selected by paediatric neuro-oncologists on patient derived DMG cell cultures identified panobinostat as a potential therapeutic option [17].

Here we conducted a large, unbiased HTS utilising biologically active, FDA-approved pharmaceutical compounds encompassing diverse activities, targets, and mechanisms of action. Through screening a panel of DMG primary cultures, we identified fenretinide as a promising therapeutic against DMG. Our findings reveal that fenretinide acts via multiple therapeutic vulnerabilities, including inhibition of PDGFRα, upregulation of the unfolded protein response (UPR)/endoplasmic reticulum (ER) stress and downregulation of neurogenesis pathways. Moreover, fenretinide demonstrates the critical ability to penetrate the blood-brain barrier (BBB), making it a promising antitumour agent for DMG treatment.

MATERIALS AND METHODS

Human DMG neurosphere-forming culture.

Primary DMG lines and murine DMG cells were grown as previously reported in Khan et al. (59) and du Chatinier et al. (60), respectively.

Inducible lentiviral PDGFR α shRNA DMG cells.

Experimental details are provided in the Supplementary information.

High-throughput screening.

A collection of 3,570 compounds from the Prestwick Chemical Library, LOPAC, and TocriScreen Total libraries was screened on SU-DIPGVI and HSJD-DIPG007 cells. Cells were seeded in 96- or 384-well plates and treated with compounds at 5µM (HSJD-DIPG007) or 10µM (SU-DIPGVI) for 72 hours. Cell viability was measured using the Alamar Blue assay and analyzed with ActivityBase software, with raw data normalized to the DMSO control. More experimental details are provided in the Supplementary information.

Proliferation assay.

The cytotoxicity assays were as outlined in Khan et al (59). Cells were seeded at 2500-3500 cells/100uL.

Soft agar colony assays.

Experimental details are provided in the Supplementary information.

Lentiviral experiments

Inducible lentiviral PDGFR α transduced RA055 cells were seeded at 800 cells/well in media containing 5% FBS with or without 2ug/mL doxycycline with or without 1.6µM fenretinide in 6-well plates and maintained for a period of 3 weeks before staining and analysis. More experimental details are provided in the Supplementary information.

Intracranial DMG cell injection, animal monitoring and endpoint.

Intracranial injections were undertaken as outlined in Khan et al. (59) and du Chatinier et al. (60). All survival study mice were monitored daily for signs of tumour development by assessing neurological and clinical symptoms. Mice exhibiting clinical signs of neurologic decline, such as ataxia, circling, and head tilting with or without 20% weight loss were humanely euthanased for histological analysis of tumours.

In vivo efficacy drug treatments.

Experimental details are provided in the Supplementary information.

Pharmacokinetic analysis of in vivo brain samples.

Experimental details are provided in the Supplementary information.

Histological analysis of brain tissue.

Experimental details are provided in Supplementary Information, while the analysis was performed using Andy's Algorithms on the image analysis pipeline FIJI (61).

Apoptosis, mitochondrial function and DNA damage assays.

Reactive oxygen species production assay

Experiments were performed using MitoSox Red staining (Thermo-Fisher) and flow cytometric analysis. Experimental details are provided in the Supplementary information.

Mitochondrial depolarisation

Experiments were performed with JC-1 staining (Thermo-Fisher) and flow cytometric analysis. Experimental details are provided in the Supplementary information.

LOcation-specific DNA Repair and Damage Quantification (LORD-Q)

Measurement of mitochondrial and nuclear DNA damage was performed using the LORD-q assay as established by literature[18]. A detailed experimental protocol is provided in the Supplementary information.

Caspase activity assay

Experimental details are provided in the Supplementary information.

Annexin V FITC/Propidium iodide assay

HSJD-DIPG007 cells were treated with fenretinide, harvested after 24-48 hours, and stained with Annexin V FITC and Propidium Iodide. Samples were analyzed using a BD FACSCanto II flow cytometer. More experimental details are provided in Supplementary Information.

Molecular analysis

Proteome profiler array

Human Phospho-RTK Array Kit from R&D systems was used as per the manufacturer's guidelines. Array was imaged using the ChemiDoc Touch Imaging System (Bio-Rad).

Protein Kinase Activity Measurement

Inhibition of protein kinase (PDGFR α) activity was investigated by using ADP-Glo Kinase Assay (Promega). Luminescence was measured with Wallac 1420 Victor2 Microplate Reader (Perkin Elmer Life Sciences).

Real-time quantitative polymerase chain reaction (qPCR)

Experimental details are provided in the Supplementary information.

Western blot analysis

Experimental details are provided in the Supplementary information.

RNA sequencing and analysis

HSJD-DIPG007 and RA055 cells were treated with fenretinide or vehicle control for 24-72 hours, followed by RNA extraction and sequencing. RNA quality was assessed using spectrophotometry and the TapeStation RNA assay. Libraries were prepared, normalized, pooled, and sequenced on the NovaSeq 6000. Reads were aligned to the human genome using STAR, quantified with RSEM, (63) and differential expression was analyzed with edgeR. Enrichment analysis of significant genes was conducted using enrichR, ranking gene sets by adjusted p-value and combined score. (64). More experimental details are provided in the Supplementary iInformation.

Statistics

Data were analyzed with GraphPad Prism 8 using an ordinary one-way ANOVA with multiple comparisons. P values less than 0.05 were considered statistically significant, and p values and statistical significance were noted on graphs when necessary. Cytotoxic assay and soft agar colony-forming assay results are displayed as average with error shown as SEM. The data from the qPCR runs were in the form of cycle threshold (Ct) values. The expression differences between samples was calculated using $2-\Delta\Delta$CT method. Survival analysis of orthotopic xenograft models was performed with MantelCox log-rank analysis.

Study Approval

All animal experiments were performed according to the Australian Code of Practice for the Care and Use of Animals for Scientific Purposes under the Animal Research Regulation of the New

South Wales (Australia) and under a protocol approved by the Animal Use and Care Committees of the University of New South Wales.

Data Availability

The data generated in this study are available upon request from the corresponding author.

RESULTS

High throughput screening identifies compounds of interest in DMG.

We performed a high throughput screen of 3,570 biologically active, clinically approved pharmaceutical compounds, each at a single concentration of 5 µM for HSJD-DIPG007 and 10 µM for SU-DIPGVI cells [19] (**Figure 1A, B**). This identified 90 drug hits that reduced DMG cell viability to less than 10% compared to untreated cells (**Supplementary Table 1)**. Of these 90 compounds, 29 were selected for further investigation based on a comprehensive literature review for each compound that suggested their potential for BBB permeation. Twenty one of the 29 compounds were excluded after validation testing showed reduced cytotoxic effects, with IC50s >10 µM against HSJD-DIPG007 and/or SU-DIPGVI cells or similar activity against DMG cells compared with non-tumour MRC5 cells (**Supplementary Table 2, Supplementary Figure 1**). Of the 8 remaining drugs, Lanatoside C was selected over digoxin (both cardiac glycosides), and mefloquine hydrochloride was selected over quinacrine dihydrochloride (both antimalarials) for further investigation due to improved performance and lower IC50 values in the validation testing.

These 6 drugs were next validated against an extended panel of DIPG cells to establish a dose-response curve and IC50 for each agent in each DIPG neurosphere culture (**Figure 1C-H**, **Supplementary Table 3**). All 6 candidate drugs exhibited cytotoxic activity in at least 6 of the 8 primary patient-derived DIPG neurosphere-forming cultures, with lower IC50s in DMG cultures in comparison with normal healthy astrocytes (NHAs) (**Supplementary Table 4**). The 6 candidate drugs were further tested in soft agar colony-forming assays. All drugs decreased colony formation in a dose-dependent manner at low micromolar concentrations in HSJD-DIPG007 cells (Supplementary Figure 2A-F), with similar findings observed across all drug candidates tested in SU-DIPGVI cells (**Supplementary Figure 2G-L**).

Validation of anti-tumour efficacy of drug candidates in DMG orthotopic animals.

In vitro activity does not always correspond with *in vivo* efficacy, particularly in DMG models where the intact BBB can prevent drug penetration into the tumour [20]. Therefore, to further prioritize the top hits, we next examined the *in vivo* efficacy of each of the 6 candidate drugs in aggressive orthotopic DMG models (**Figure 2**). We did not observe any significant weight loss or other evidence of systemic toxicity associated with any individual drug treatments (**Supplementary Figure 3**). Treatment with LYM-X-SORB-fenretinide, a formulation designed to improve intestinal absorption, led to significant survival benefits (**Figure 2C**) (median survival of vehicle 53 days vs fenretinide 58 days, p=0.009) and a significant decrease in Ki67 positive staining (p=0.0393) (**Figure 2D**) [21]. In contrast, lanatoside C, ivermectin, SAHA, mefloquine hydrochloride and parthenolide treatments showed no improvement in survival compared to vehicle-treated controls. (**Figure 2A-B, F-H, Supplementary Figure 4)**. To understand why these active agents failed to improve survival *in vivo*, we next measured the intra-tumoural

concentrations of each compound in each *in vivo* model (**Supplementary Figure 4)**). While brain penetration was confirmed through LC-MS/MS analysis for fenretinide and mefloquine hydrochloride (**Figure 2E**, **Supplementary Figure 4E**) lanatoside C, ivermectin, SAHA and parthenolide each failed to penetrate the BBB with undetectable drug concentrations in brain and tumour tissue (**Supplementary Figure 4A-B, D, F**).

Fenretinide is the only active retinoid when tested in DMG cells.

Fenretinide belongs to a class of compounds called 'retinoids,' some of which are commonly used in children and in other childhood cancers [22,23]. We, therefore, sought to establish whether the highly potent effect of fenretinide against DIPG was a class effect that could be extended to other retinoids. Cytotoxicity assays performed in both SU-DIPGVI and HSJD-DIPG007 cells, using 9-cis retinoic acid, 13-cis retinoic acid, ATRA and fenretinide, revealed that the potent cytotoxicity was specific to fenretinide. Treatment with other retinoids did not affect tumour cell viability, even at concentrations greater than 10 µM in both HSJD-DIPG007 and SU-DIPGVI cells (**Supplementary Figure 5A, B**).

Fenretinide induces the production of reactive oxygen species (ROS), caspase activation and apoptosis in HSJD-DIPG007 cells *in vitro.*

Fenretinide has been shown to induce apoptosis by stimulating signalling molecules such as ceramide [24] and caspases [25], as well as elevating ROS levels [26]. To investigate whether fenretinide induces ROS production and, subsequently, apoptosis in DMG, a MitoSOX Red assay was used to assess ROS levels. Fenretinide treatment led to potent ROS production in DMG cells starting

as early as 1 hour following treatment (**Figure 3A**). Using JC-1 staining, we assessed mitochondrial depolarization in fenretinide-treated DIPG cells and observed a significant reduction in the red/green fluorescence ratio, indicative of impaired mitochondrial integrity in two primary DMG cultures (**Supplementary Figure 6A/B**). Consistent with previous studies, fenretinide treatment resulted in a significant increase in phospho-H2AX levels, indicating activation of the DNA damage response in two DMG cultures (**Supplementary Figure 6C/D**). Given the observed increase in ROS production and phospho-H2AX levels, we hypothesized that fenretinide-induced oxidative stress might directly contribute to DNA damage. To investigate this, we employed the LOcation-specific DNA Repair and Damage Quantification (LORD-Q) assay, which estimates DNA damage rates through real-time polymerase chain reaction (PCR)[18]. DNA damage is quantified by observing changes in the delta Ct (ΔCt) between long and short DNA fragments during PCR amplification. Interestingly, fenretinide did not induce detectable mitochondrial or nuclear DNA damage in HSJD-DIPG007 cells after 24 or 48 hours of treatment. In contrast, RA055 cells showed a significant increase in nuclear DNA lesions and a decrease in mitochondrial DNA lesions after 48 hours, highlighting cell line-specific effects (**Supplementary Figure 6E/F**). It is important to note that our assessment was limited to the *COL1A1* gene, and damage may occur in other genes that were not evaluated in this study. To further understand the effect of fenretinide on the induction of apoptosis, we next investigated the activation of caspases in DMG cells. Treatment with fenretinide led to significant increases in caspase 3/7, caspase 8 and caspase 9, indicating induction of both intrinsic and extrinsic apoptotic pathways (**Figure 3B, Supplementary Figure 7A/B**). Fenretinide treatment subsequently increased protein levels of cleaved caspase and cleaved PARP protein expression over time (**Figure 3C, Supplementary Figure 6G-J**). The effect on apoptosis occurred in a dose-dependent manner as measured by the

impact of fenretinide on Annexin-V and 7AAD staining (**Figure 3D**). Similarly, we evaluated the effects of fenretinide treatment in murine glioma cells (H3K27M). Fenretinide was similarly cytotoxic as primary DMG cells and enhanced DNA damage response PH2AX and apoptotic markers cleaved caspase 3 and cleaved PARP (**Supplementary Figure 8A-H**).

Fenretinide inhibits PDGFRα in DMG cells.

Since fenretinide has previously been shown to affect kinases such as FAK [27] and mTOR [28], we next sought to investigate whether it can affect receptor tyrosine kinases in DMG. We first evaluated whether fenretinide affects the phosphorylation status of receptor tyrosine kinases using a 96-well phospho-kinase array as previously described [29]. Fenretinide treatment significantly reduced phospho-PDGFRα signal intensities compared to untreated HSJD-DIPG007 cells (**Supplementary Figure 9)**. Western blotting analysis confirmed significant decreases in levels of total and phospho-PDGFRα (**Figure 3E, Supplementary Figure 10A-C**) but no changes in PI3K, AKT and mTOR following treatment with 2μM of fenretinide at 48 hours (**Supplementary Figure 10D-K**). Given the effect of fenretinide on both total and phospho-PDGFRα, we next assessed whether fenretinide acts as a direct kinase inhibitor. Protein kinase activity measurement assays were thus employed using the ADP-Glo kinase assay. We found that fenretinide did not affect PDGFRα activity through direct binding compared to the established PDGFR inhibitor, ponatinib, as a positive control (**Supplementary Figure 11**). Therefore, to investigate whether the effect on PDGFRα occurs at the transcriptional level, we evaluated *PDGFRA* mRNA expression levels by real-time qPCR. Compared to untreated cells, *PDGFRA* mRNA expression levels were significantly lower in fenretinide-treated DMG cells at both 24 and 48 hours (**Figure 3F**). Together, these results suggest that fenretinide does not directly target kinase activity but inhibits

PDGFRA through suppression of gene transcription. Given the effect on *PDGFRA* gene transcription, we next sought to determine whether fenretinide affected epigenetic drivers. We found that fenretinide treatment increased H3K27 acetylation, trimethylation at 24 and 48h and total H3 levels in total protein lysates at 48 hours (**Figure 3G, Supplementary Figure 12A-C)** with no changes observed when examined in nuclear histone extracts (**Supplementary Figure 13A).** Similarly, total lysates from murine glioma cells treated with fenretinide exhibited significantly higher levels of H3K27 trimethylation and total H3 levels (**Supplementary Figure 13B-E**).

Given the effects of fenretinide on *PDGFRA* gene expression and protein levels, we sought to investigate its effects on *PDGFRA* over-expressing RA055 DMG cells. Western blotting analysis confirmed an increase in cleaved parp and caspase (**Figure 3H, Supplementary Figure 14**) and a decrease in p-PDGFRα and p-PI3Kp85 when treated with 4 μM fenretinide at 24 and 48 hours (**Figure 3I, Supplementary Figure 15, Supplementary Figure 16**). However, no downstream effects were seen on AKT or mTOR (**Supplementary Figure 16**). Similar to results shown in HSJD-DIPG007 cells, fenretinide treatment increased H3K27 acetylation, trimethylation and total H3 in total protein lysates at 24 and 48 hours in PDGFRα-amplified RA055 DMG cells (**Figure 3J, Supplementary Figure 17).** To validate whether fenretinide exerts its effect at least in part through PDGFRα inhibition and whether its activity could be enhanced with further PDGFRα suppression, we performed knockdown experiments. Knockdown of PDGFRα in RA055 cells using doxycycline-inducible shRNA significantly decreased colony formation, which was further enhanced by treatment with fenretinide (**Supplementary Figure 18**).

Fenretinide treatment upregulates the ER stress and UPR pathways whilst also downregulating neurogenesis.

Given that fenretinide affects *PDGFRA* at the transcriptional level, and that fenretinide was active across the broader DMG panel, and that fenretinide was active in cells without PDGFRA as a driver, we next sought to determine the broader impact of fenretinide on the transcriptome through bulk RNA-sequencing. Significant gene expression changes were observed in both HSJD-DIPG007 and RA055 (PDGFRα amplified) cultures when treated with fenretinide for 24 hours **(Supplementary Figure 19, 20).** Gene ontology (GO) enrichment analysis of biological processes performed on the upregulated genes showed enrichment and a high number of genes in gene sets related to ER stress and the UPR in both HSJD-DIPG007 and RA055. (**Figure 4A, Supplementary Figure 21)**. Gene expression analysis confirmed increased expression of UPR components *ATF4* (**Figure 4B**), *CHOP* (**Figure 4C**), *BIP* (**Figure 4D**) and *XBP1* (**Figure 4E**), with levels of both *CHOP* and *BIP* reaching statistical significance in HSJD-DIPG007 cells (**Figure 4C, E;** p=0.0156, p=0.0096 respectively) but not RA055 cells. Protein analysis confirmed a significant increase in CHOP, BiP and XPB1 in HSJD-DIPG007 and ATF4, CHOP, BiP and XPB1 RA055 cells after 24 hours of treatment with fenretinide **(Supplementary Figure 22).** To examine whether these effects were independent of, or occurred secondary to induction of ROS, we tested the impact of antioxidant supplementation. Treatment with neither n-acetylcysteine (NAC) nor Mito-tempo inhibited fenretinide-induced UPR-mediated cell death (**Supplementary Figure 23),** suggesting an independent effect.

GO enrichment analysis of biological processes performed on the downregulated genes showed enrichment with an overlap of significant genes in gene sets related to neurogenesis in both the

HSJD-DIPG007 and RA055 cells (**Figure 5A, Supplementary Figure 24).** Gene expression analysis confirmed significantly decreased levels of *ASCL1*, *OLIG2*, and *DLL1* in RA055 cells (p=0.009, p=0.0076, p=0.0117 respectively, **Figure 5B, G, H**), with *ASCL1* also significantly decreased in HSJD-DIPG007 cells (p=0.0013, **Figure 5B**). No significant changes in gene expression were observed in DIPG007 or RA55 cells in NOTCH1, HES1, LEF1 or NESTIN (**Figure 5C-F**) Proteomic analysis confirmed a significant decrease in ASCL1, C-Notch1, Notch1 and Olig2 in HSJD-DIPG007 and APC, ASCL1, C-Notch1, Notch1, LEF1, Nestin, Olig2 and DLL1 in RA055 cells after 24 hours treatment with fenretinide **(Supplementary Figure 25).** Together these results suggest a disparate effect of fenretinide on ER stress, UPR and neurogenesis pathways.

Fenretinide treatment upregulates the mitophagy and autophagy.

Pathways related to mitochondrial dysfunction, including mitophagy, were identified, supporting ROS-mediated effects of fenretinide (Supplementary Table 5). Gene expression analysis revealed cell line-specific responses to treatment. In RA055 cells, mitophagy-related markers such as *PARKIN* expression increased significantly after 48 hours, while *PINK1* remained unchanged. HSJD-DIPG007 cells showed no changes in *PARKIN* or *PINK1* expression (**Supplementary Figure 26 A/B**). Autophagy markers in RA055 cells showed elevated *WIPI1*, *LC3*, and *SQSTM1* expression, whereas HSJD-DIPG007 cells exhibited increased *LC3* and *SQSTM1* but no changes in *WIPI1* (**Supplementary Figure 26 C-E**). Proteomic analysis confirmed significant effects in HSJD-DIPG007 at 48 hours, with increased levels of PARKIN, LC3A/B, WIPI1, and SQSTM1 (**Supplementary Figure 27 A-F**). In RA055 cells, PINK1 and WIPI1 showed changes at 48 hours,

with no alterations in other mitophagy or autophagy mediators at the protein level (**Supplementary Figure 27 G-K**).

Fenretinide is active *in vivo* in PDGFRα-amplified DMG models.

We next sought to examine the *in vivo* efficacy of fenretinide in PDGFRα-amplified RA055 DMG orthotopic models using two different formulations (LYM-X-SORB and nanomicellar fenretinide). The LYM-X-SORB-fenretinide formulation was designed to improve the intestinal absorption of fenretinide as described previously [21]. The nanomicellar fenretinide formulation has been more recently developed to allow a nano-targeted delivery of fenretinide [30] to solid tumours. RA055 engrafted mice were treated with vehicle control or fenretinide formulations. The median survival was 48 days for vehicle-treated, and LYM-X-SORB fenretinide-treated mice showed a significant survival benefit with a median survival of 60 days (P= 0.0149) compared to vehicle-treated mice (**Figure 6A**). RA055 engrafted mice were treated with nanomicelle control and nanomicellar fenretinide. The median survival was significantly enhanced in nanomicellar fenretinide-treated mice with a median survival of 66 days compared to 55 days in the nanomicelle control (p=0.0264) (**Figure 6B**). In addition, we employed an immunocompetent murine model of DMG featuring a constitutively active PDGFRa to assess the efficacy of the LYM-X-SORB-fenretinide formulation. Our findings revealed a significant increase in median survival for animals treated with fenretinide (58 days) compared to the vehicle-treated group (54 days, P=0.0082) (**Figure 6C**). Pharmacokinetic analysis further validated the presence of fenretinide in the brains of the engrafted animals (**Figure 6D**). The observed differences in drug levels between the PDX and transgenic models, despite moderate efficacy in both, may be attributed to their distinct tumour growth patterns, with PDX models showing diffuse growth similar to patient biopsies and

transgenic models displaying a glioblastoma-like structure with densely packed, highly nuclear regions[31].

Ki-67 staining confirmed the presence of tumour cells in the brainstem of intracranially injected mice, with a significant decrease ($p<0.0001$) in Ki67 staining observed in the brains of mice treated with LYM-X-SORB fenretinide (**Figure 6E, Supplementary Figure 28A**) or nanomicellar fenretinide ($p=0.0003$) (**Figure 6F, Supplementary Figure 28E**). However, no significant changes were observed in cleaved caspase-3 staining with either fenretinide formulation (**Supplementary Figure 29A/B, Supplementary Figure 28B,F**).

PDGFRα quantification with immunohistochemistry confirmed that treatment with fenretinide inhibited PDGFR expression *in vivo*, with a significant reduction in PDGFRα-positive cells observed in the brains of mice treated with LYM-X-SORB fenretinide ($p=0.0053$) (**Figure 6G, Supplementary Figure 28C**) and a significant decrease in mice treated with nanomicellar fenretinide ($p=0.014$) (**Figure 6H, Supplementary Figure 28G**). These findings demonstrate the antitumour efficacy of both fenretinide formulations and their potential as brain penetrant modalities for targeting PDGFRα in a PDGFRα-amplified DMG model. Further immunohistochemical analysis revealed that neither fenretinide formulation restored H3K27me3 levels in the RA055 PDX model (**Supplementary Figure 28D,H, Supplementary Figure 29C,D**). Similarly, no effects on trimethylation were observed in the HSJD-DIP007 PDX model following LYM-X-SORB fenretinide treatment **(Supplementary Figure 30**).

Fenretinide combination with irradiation does not enhance therapeutic benefit in vivo.

Given that radiotherapy is currently the only standard therapeutic option for DMG patients, we evaluated whether combining it with fenretinide could enhance its effectiveness. Clonogenic assays were performed in HSJD-DIPG007 cells, treating them with a low dose of fenretinide (0.2 µM) and 2 Gy irradiation. The combination treatment resulted in a significantly lower number of colonies compared to the individual treatments (**Supplementary Figure 31A**). Building on these promising findings, we assessed the therapeutic efficacy of the LYM-X-SORB fenretinide formulation in combination with irradiation in the HSJD-DIPG007 orthotopic DMG model. Engrafted mice were divided into four treatment groups: vehicle control, LYM-X-SORB fenretinide formulation, irradiation (8 Gy), and the combination. The median survival for vehicle-treated mice was 53 days, while LYM-X-SORB fenretinide-treated mice showed a median survival of 58 days, as previously reported ($p=0.009$). Although the irradiation-treated group demonstrated improved survival (65 days, $p<0.0001$ vs. vehicle), the combination therapy did not result in further survival benefit (61 days) (**Supplementary Figure 31B**).

DISCUSSION

Active treatments are urgently needed for DMG. HTS allows the evaluation of large numbers of pharmaceutical compounds with various biological activities, targets, and mechanisms of action. A considerable advantage of using an HTS approach is that it does not rely on inhibiting known oncogenic targets and can potentially unveil novel targets for further investigation. However, one of the limitations is that it is primarily an *in vitro* technique that does not consider the many barriers and interactions that occur *in vivo*. Such screening has been used to identify therapies for other

cancers [32,33], but limited screening has been undertaken to date for DMG [34]. We have identified potential novel therapies using our DMG cell panel *in vitro* and our unique *in vivo* animal models.

Of the six HTS drug hits, we found that five drugs - lanatoside C, ivermectin, SAHA, mefloquine hydrochloride and parthenolide, despite showing *in vitro* activity, had no impact on animal survival and cellular proliferation. Previous *in vitro* studies have demonstrated that lanatoside C [35-37], ivermectin [38-40], SAHA [41], mefloquine hydrochloride [42] and parthenolide [43] all have anticancer potential due to their mechanisms of action and molecular pathways targets. Lanatoside C [44] and ivermectin [38,45] have been examined in glioblastoma (GBM), nevertheless the employment of subcutaneous models did not allow for testing of BBB permeability. Parthenolide has previously been examined in an orthotopic GBM model, decreasing tumour volume, however, the effect on overall survival was not reported [46]. Despite the strong in vitro activity and sufficient levels of mefloquine in animal brains, we observed no therapeutic efficacy. This lack of efficacy may be attributed to the absence of key targets identified for mefloquine, such as beta-catenin[47], lysosomes[48], and lipid peroxidation (LPCAT3)[49] in the *in vivo* setting. The absence of these targets in the animal models could explain the failure to translate the observed in vitro effect into a therapeutic benefit. Generally, we demonstrated that the lack of therapeutic efficacy observed *in vivo* is likely due to an inability to achieve sufficient drug concentration in the tumour to have a potent effect. These comprehensive negative results highlight the intact BBB as a key mechanism of failure of therapies in DMG, and the necessity of comprehensive pre-clinical testing *in vitro* and *in vivo* before clinical trials are initiated.

Fenretinide is a semi-synthetic retinoid derivative with potential antineoplastic and chemo-preventive activities [28,50], and a previous study has shown *in vivo* efficacy in medulloblastoma [51]. We found that fenretinide significantly increased survival in two orthotopic patient-derived DMG animal models and one immunocompetent DMG model using two unique formulations of fenretinide (LYM-X-SORB and nanomicellar fenretinide), indicating that fenretinide can penetrate the BBB and is active in DMG. Similar to reports in other cancer types, we showed that treatment with fenretinide increased ROS production and induced mitochondrial depolarisation and apoptosis in DMG cells [26,52,53]. Our experiments have uncovered new mechanisms of action for fenretinide. We found that treatment with fenretinide inhibits PDGFRα gene expression, protein and phosphorylation levels. We confirmed that fenretinide upregulates ER stress and UPR [54-56] autophagy and concurrently identified a novel downregulation of neurogenesis. Furthermore, we confirmed that fenretinide is also effective in DMG models exhibiting PDGFRα amplification, a driver that can result in resistance to RTK inhibitors [57]. The loss of H3K27 trimethylation, driven by the H3K27M mutation, is a hallmark of DMG tumours. *In vitro*, fenretinide treatment led to a significant increase in H3K27me3, likely linked to higher total H3 levels. However, RNA sequencing did not show upregulation of histone-related genes, suggesting the change is not due to new histone synthesis. A possible explanation is histone leakage from the nucleus into the cytoplasm, forming micronuclei with altered H3K27me3[58]. Further studies are needed to explore whether these changes reflect a stress response or a role for histones as danger signals[59]. *In vivo*, fenretinide treatment did not result in significant changes, indicating that the drug concentrations reaching the brain may not induce strong epigenetic effects.

Recently Filbin *et al.* [10] found that H3K27M mutant gliomas contain cells that resemble oligodendrocyte precursor cells (OPC), which exhibit greater proliferation and tumour-propagating potential than their more differentiated counterparts and are in part sustained by PDGFRα signalling. This suggests that the oligodendrocyte precursor like cells are the predominant subpopulation of H3K27M tumours and may be susceptible to therapeutic strategies that target lineage-defined cellular programs such as PDGFRα [10]. Although our experiments indicate effective targeting of PDGFRα, further experiments may determine if fenretinide can directly influence OPC-like cells.

Retinoid compounds and their synthetic analogues have long been studied as possible anticancer agents in clinical trials for adult and paediatric malignancies [60]. However, vitamin-A-associated toxicity has limited its long-term use, thus, other compounds with reduced side effects have been developed, such as fenretinide [60]. Multiple studies have indicated that fenretinide has an improved toxicity profile with accumulation in fatty tissues such as adipose tissue, mammary gland and brain rather than the liver [61,62]. We have shown that fenretinide is a PDGFRα inhibitor with BBB permeability with promise for clinical translation. Until recently, clinical trials of PDGFR inhibitors in CNS tumours have failed due to toxicity, low BBB permeability and limited accumulation at the tumour site [63,64]. PDGFRα inhibitor avapritinib is currently in a clinical trial (NCT04773782) and has demonstrated high BBB penetration making it a promising therapeutic for CNS tumours, supported by case reports suggesting some clinical activity in DMG [65]. Unfortunately, in our studies, combining fenretinide with irradiation did not offer any additional survival benefit over either treatment alone. Future studies are needed to determine whether this potential therapeutic efficacy can be enhanced through combinatorial strategies. Transcriptomic

analyses, such as bulk RNA-seq or single-cell RNA-seq in the brains from DMG PDX or transgenic models, would be beneficial in identifying further mechanisms of action, assessing the effects on the microenvironment and determining synergistic combinations.

Here we utilised a diverse panel of DMG primary cultures for high-throughput drug screening, revealing the critical impact of blood-brain barrier (BBB) permeability on drug efficacy *in vivo*. Among the identified compounds, fenretinide emerged as a drug that warrants further investigation as a potential combination therapy for DMG. Mechanistic studies demonstrated that fenretinide enhanced apoptotic cell death by inhibiting PDGFRα transcription, leading to downregulation of PDGFRa, increasing ROS production, with induction of apoptosis, increasing ER stress, UPR and downregulating neurogenesis, revealing new oncogenic dependencies in this disease. Notably, fenretinide represents a novel treatment approach targeting PDGFRα in DMG, overcoming the limitation of many PDGFR inhibitors with poor BBB penetration. With its BBB permeability and potent anti-DMG activity, fenretinide holds promising clinical potential as a PDGFRα inhibitor for the treatment of DMG.

References

1. Lapin DH, Tsoli M, Ziegler DS. Genomic Insights into Diffuse Intrinsic Pontine Glioma. *Front Oncol.* 2017; 7:57.
2. Freeman CR, Farmer JP. Pediatric brain stem gliomas: a review. *Int J Radiat Oncol Biol Phys.* 1998; 40(2):265-271.
3. Khuong-Quang D-A, Buczkowicz P, Rakopoulos P, et al. K27M mutation in histone H3. 3 defines clinically and biologically distinct subgroups of pediatric diffuse intrinsic pontine gliomas. *Acta neuropathologica.* 2012; 124(3):439-447.
4. Wu G, Broniscer A, McEachron TA, et al. Somatic histone H3 alterations in pediatric diffuse intrinsic pontine gliomas and non-brainstem glioblastomas. *Nature genetics.* 2012; 44(3):251.
5. Wu G, Diaz AK, Paugh BS, et al. The genomic landscape of diffuse intrinsic pontine glioma and pediatric non-brainstem high-grade glioma. *Nature genetics.* 2014; 46(5):444.
6. Puget S, Philippe C, Bax DA, et al. Mesenchymal transition and PDGFRA amplification/mutation are key distinct oncogenic events in pediatric diffuse intrinsic pontine gliomas. *PloS one.* 2012; 7(2).
7. Paugh BS, Zhu X, Qu C, et al. Novel oncogenic PDGFRA mutations in pediatric high-grade gliomas. *Cancer research.* 2013; 73(20):6219-6229.
8. Paugh BS, Broniscer A, Qu C, et al. Genome-wide analyses identify recurrent amplifications of receptor tyrosine kinases and cell-cycle regulatory genes in diffuse intrinsic pontine glioma. *J Clin Oncol.* 2011; 29(30):3999-4006.
9. Wu G, Diaz AK, Paugh BS, et al. The genomic landscape of diffuse intrinsic pontine glioma and pediatric non-brainstem high-grade glioma. *Nat Genet.* 2014; 46(5):444-450.
10. Filbin MG, Tirosh I, Hovestadt V, et al. Developmental and oncogenic programs in H3K27M gliomas dissected by single-cell RNA-seq. *Science.* 2018; 360(6386):331-335.

11. Vanan MI, Eisenstat DD. DIPG in Children – What Can We Learn from the Past? *Frontiers in Oncology.* 2015; 5(237).

12. Veringa SJ, Biesmans D, van Vuurden DG, et al. In vitro drug response and efflux transporters associated with drug resistance in pediatric high grade glioma and diffuse intrinsic pontine glioma. *PloS one.* 2013; 8(4).

13. Pollack IF, Jakacki RI, Blaney SM, et al. Phase I trial of imatinib in children with newly diagnosed brainstem and recurrent malignant gliomas: a Pediatric Brain Tumor Consortium report. *Neuro Oncol.* 2007; 9(2):145-160.

14. Broniscer A, Baker SD, Wetmore C, et al. Phase I trial, pharmacokinetics, and pharmacodynamics of vandetanib and dasatinib in children with newly diagnosed diffuse intrinsic pontine glioma. *Clin Cancer Res.* 2013; 19(11):3050-3058.

15. Ashburn TT, Thor KB. Drug repositioning: identifying and developing new uses for existing drugs. *Nature reviews Drug discovery.* 2004; 3(8):673-683.

16. Halvorson KG, Barton KL, Schroeder K, et al. A high-throughput in vitro drug screen in a genetically engineered mouse model of diffuse intrinsic pontine glioma identifies BMS-754807 as a promising therapeutic agent. *PLoS One.* 2015; 10(3):e0118926.

17. Grasso CS, Tang Y, Truffaux N, et al. Functionally defined therapeutic targets in diffuse intrinsic pontine glioma. *Nat Med.* 2015; 21(6):555-559.

18. Dannenmann B, Lehle S, Lorscheid S, Huber SM, Essmann F, Schulze-Osthoff K. Simultaneous quantification of DNA damage and mitochondrial copy number by long-run DNA-damage quantification (LORD-Q). *Oncotarget.* 2017; 8(68):112417-112425.

19. Ehteda A, Simon S, Franshaw L, et al. Dual targeting of the epigenome via FACT complex and histone deacetylase is a potent treatment strategy for DIPG. *Cell Reports.* 2021; 35(2):108994.

20. Warren KE. Beyond the Blood:Brain Barrier: The Importance of Central Nervous System (CNS) Pharmacokinetics for the Treatment of CNS Tumors, Including Diffuse Intrinsic Pontine Glioma. *Front Oncol.* 2018; 8:239.

21. Cooper JP, Reynolds CP, Cho H, Kang MH. Clinical development of fenretinide as an antineoplastic drug: Pharmacology perspectives. *Exp Biol Med (Maywood).* 2017; 242(11):1178-1184.

22. Villablanca JG, Krailo MD, Ames MM, Reid JM, Reaman GH, Reynolds CP. Phase I trial of oral fenretinide in children with high-risk solid tumors: a report from the Children's Oncology Group (CCG 09709). *J Clin Oncol.* 2006; 24(21):3423-3430.

23. Maurer BJ, Kang MH, Villablanca JG, et al. Phase I trial of fenretinide delivered orally in a novel organized lipid complex in patients with relapsed/refractory neuroblastoma: a report from the New Approaches to Neuroblastoma Therapy (NANT) consortium. *Pediatr Blood Cancer.* 2013; 60(11):1801-1808.

24. Morad SAF, Davis TS, Kester M, Loughran TP, Jr., Cabot MC. Dynamics of ceramide generation and metabolism in response to fenretinide--Diversity within and among leukemia. *Leuk Res.* 2015; 39(10):1071-1078.

25. Puduvalli VK, Saito Y, Xu R, Kouraklis GP, Levin VA, Kyritsis AP. Fenretinide activates caspases and induces apoptosis in gliomas. *Clin Cancer Res.* 1999; 5(8):2230-2235.

26. Cuperus R, Leen R, Tytgat GA, Caron HN, van Kuilenburg AB. Fenretinide induces mitochondrial ROS and inhibits the mitochondrial respiratory chain in neuroblastoma. *Cell Mol Life Sci.* 2010; 67(5):807-816.

27. Han BB, Li S, Tong M, et al. Fenretinide Perturbs Focal Adhesion Kinase in Premalignant and Malignant Human Oral Keratinocytes. Fenretinide's Chemopreventive Mechanisms Include ECM Interactions. *Cancer Prev Res (Phila).* 2015; 8(5):419-430.

28. Orienti I, Francescangeli F, De Angelis ML, et al. A new bioavailable fenretinide formulation with antiproliferative, antimetabolic, and cytotoxic effects on solid tumors. *Cell Death & Disease.* 2019; 10(7):529.

29. Rani S, O'Driscoll L. Analysis of Changes in Phosphorylation of Receptor Tyrosine Kinases: Antibody Arrays. In: Germano S, ed. *Receptor Tyrosine Kinases: Methods and Protocols*. New York, NY: Springer New York; 2015:15-23.

30. Orienti I, Farruggia G, Nguyen F, et al. Nanomicellar Lenalidomide-Fenretinide Combination Suppresses Tumor Growth in an MYCN Amplified Neuroblastoma Tumor. *Int J Nanomedicine.* 2020; 15:6873-6886.

31. du Chatinier A, Meel MH, Das AI, et al. Generation of immunocompetent syngeneic allograft mouse models for pediatric diffuse midline glioma. *Neurooncol Adv.* 2022; 4(1):vdac079.

32. Atkinson Jennifer M, Shelat Anang A, Carcaboso Angel M, et al. An Integrated In Vitro and In Vivo High-Throughput Screen Identifies Treatment Leads for Ependymoma. *Cancer Cell.* 2011; 20(3):384-399.

33. Gupta PB, Onder TT, Jiang G, et al. Identification of Selective Inhibitors of Cancer Stem Cells by High-Throughput Screening. *Cell.* 2009; 138(4):645-659.

34. Lin GL, Wilson KM, Ceribelli M, et al. Therapeutic strategies for diffuse midline glioma from high-throughput combination drug screening. *Science Translational Medicine.* 2019; 11(519):eaaw0064.

35. Hu Y, Yu K, Wang G, et al. Lanatoside C inhibits cell proliferation and induces apoptosis through attenuating Wnt/beta-catenin/c-Myc signaling pathway in human gastric cancer cell. *Biochem Pharmacol.* 2018; 150:280-292.

36. Durmaz I, Guven EB, Ersahin T, Ozturk M, Calis I, Cetin-Atalay R. Liver cancer cells are sensitive to Lanatoside C induced cell death independent of their PTEN status. *Phytomedicine.* 2016; 23(1):42-51.

37. Chao M-W, Chen T-H, Huang H-L, et al. Lanatoside C, a cardiac glycoside, acts through protein kinase Cδ to cause apoptosis of human hepatocellular carcinoma cells. *Scientific Reports.* 2017; 7(1):46134.

38. Liu Y, Fang S, Sun Q, Liu B. Anthelmintic drug ivermectin inhibits angiogenesis, growth and survival of glioblastoma through inducing mitochondrial dysfunction and oxidative stress. *Biochemical and Biophysical Research Communications.* 2016; 480(3):415-421.

39. Dou Q, Chen H-N, Wang K, et al. Ivermectin induces cytostatic autophagy by blocking the PAK1/Akt axis in breast cancer. *Cancer research.* 2016; 76(15):4457-4469.

40. Juarez M, Schcolnik-Cabrera A, Dueñas-Gonzalez A. The multitargeted drug ivermectin: from an antiparasitic agent to a repositioned cancer drug. *Am J Cancer Res.* 2018; 8(2):317-331.

41. Lohitesh K, Saini H, Srivastava A, Mukherjee S, Roy A, Chowdhury R. Autophagy inhibition potentiates SAHA-mediated apoptosis in glioblastoma cells by accumulation of damaged mitochondria. *Oncol Rep.* 2018; 39(6):2787-2796.

42. Liu Y, Chen S, Xue R, Zhao J, Di M. Mefloquine effectively targets gastric cancer cells through phosphatase-dependent inhibition of PI3K/Akt/mTOR signaling pathway. *Biochemical and Biophysical Research Communications.* 2016; 470(2):350-355.

43. Anderson KN, Bejcek BE. Parthenolide induces apoptosis in glioblastomas without affecting NF-kappaB. *Journal of pharmacological sciences.* 2008; 106(2):318-320.

44. Badr CE, Wurdinger T, Nilsson J, et al. Lanatoside C sensitizes glioblastoma cells to tumor necrosis factor-related apoptosis-inducing ligand and induces an alternative cell death pathway. *Neuro-oncology.* 2011; 13(11):1213-1224.

45. Song D, Liang H, Qu B, et al. Ivermectin inhibits the growth of glioma cells by inducing cell cycle arrest and apoptosis in vitro and in vivo. *J Cell Biochem.* 2019; 120(1):622-633.

46. Nakabayashi H, Shimizu K. Involvement of Akt/NF-κB pathway in antitumor effects of parthenolide on glioblastoma cells in vitro and in vivo. *BMC Cancer.* 2012; 12(1):453.

47. Li YH, Yang SL, Zhang GF, et al. Mefloquine targets beta-catenin pathway and thus can play a role in the treatment of liver cancer. *Microb Pathog.* 2018; 118:357-360.

48. Das S, Dielschneider R, Chanas-LaRue A, Johnston JB, Gibson SB. Antimalarial drugs trigger lysosome-mediated cell death in chronic lymphocytic leukemia (CLL) cells. *Leuk Res.* 2018; 70:79-86.

49. Tao Q, Liu N, Wu J, Chen J, Chen X, Peng C. Mefloquine enhances the efficacy of anti-PD-1 immunotherapy via IFN-gamma-STAT1-IRF1-LPCAT3-induced ferroptosis in tumors. *J Immunother Cancer.* 2024; 12(3).

50. Cooper JP, Reynolds CP, Cho H, Kang MH. Clinical development of fenretinide as an antineoplastic drug: Pharmacology perspectives. *Exp Biol Med (Maywood).* 2017; 242(11):1178-1184.

51. Bassani B, Bartolini D, Pagani A, et al. Fenretinide (4-HPR) Targets Caspase-9, ERK 1/2 and the Wnt3a/β-Catenin Pathway in Medulloblastoma Cells and Medulloblastoma Cell Spheroids. *PLOS ONE.* 2016; 11(7):e0154111.

52. Lovat PE, Corazzari M, Goranov B, Piacentini M, Redfern CP. Molecular mechanisms of fenretinide-induced apoptosis of neuroblastoma cells. *Ann N Y Acad Sci.* 2004; 1028:81-89.

53. Rehman F, Shanmugasundaram P, Schrey MP. Fenretinide stimulates redox-sensitive ceramide production in breast cancer cells: potential role in drug-induced cytotoxicity. *British Journal of Cancer.* 2004; 91(10):1821-1828.

54. Anding AL, Jones JD, Newton MA, Curley RW, Jr., Clagett-Dame M. 4-HPR Is an Endoplasmic Reticulum Stress Aggravator and Sensitizes Breast Cancer Cells Resistant to TRAIL/Apo2L. *Anticancer Res.* 2018; 38(8):4403-4416.

55. Lai WL, Wong NS. The PERK/eIF2 alpha signaling pathway of Unfolded Protein Response is essential for N-(4-hydroxyphenyl)retinamide (4HPR)-induced cytotoxicity in cancer cells. *Exp Cell Res.* 2008; 314(8):1667-1682.

56. Kadara H, Lacroix L, Lotan D, Lotan R. Induction of endoplasmic reticulum stress by the pro-apoptotic retinoid N-(4-hydroxyphenyl)retinamide via a reactive oxygen species-dependent mechanism in human head and neck cancer cells. *Cancer Biol Ther.* 2007; 6(5):705-711.

57. Chen Y-f, Fu L-w. Mechanisms of acquired resistance to tyrosine kinase inhibitors. *Acta Pharmaceutica Sinica B.* 2011; 1(4):197-207.

58. Agustinus AS, Al-Rawi D, Dameracharla B, et al. Epigenetic dysregulation from chromosomal transit in micronuclei. *Nature.* 2023; 619(7968):176-183.

59. Hadnagy A, Beaulieu R, Balicki D. Histone tail modifications and noncanonical functions of histones: perspectives in cancer epigenetics. *Mol Cancer Ther.* 2008; 7(4):740-748.

60. Dobrotkova V, Chlapek P, Mazanek P, Sterba J, Veselska R. Traffic lights for retinoids in oncology: molecular markers of retinoid resistance and sensitivity and their use in the management of cancer differentiation therapy. *BMC Cancer.* 2018; 18(1):1059.

61. Mehta RG, Moon RC, Hawthorne M, Formelli F, Costa A. Distribution of fenretinide in the mammary gland of breast cancer patients. *Eur J Cancer.* 1991; 27(2):138-141.

62. McIlroy GD, Delibegovic M, Owen C, et al. Fenretinide treatment prevents diet-induced obesity in association with major alterations in retinoid homeostatic gene expression in adipose, liver, and hypothalamus. *Diabetes.* 2013; 62(3):825-836.

63. Nabors LB, Supko JG, Rosenfeld M, et al. Phase I trial of sorafenib in patients with recurrent or progressive malignant glioma. *Neuro-oncology.* 2011; 13(12):1324-1330.

64. Wetmore C, Daryani VM, Billups CA, et al. Phase II evaluation of sunitinib in the treatment of recurrent or refractory high-grade glioma or ependymoma in children: a children's Oncology Group Study ACNS1021. *Cancer Med.* 2016; 5(7):1416-1424.

65. Mayr L, Trissal M, Schwark K, et al. DDDR-22. Translation of the PDGFRA/KIT inhibitor Avapritinib for pediatric High-Grade Glioma. *Neuro-Oncology.* 2022; 24(Supplement_7):vii103-vii103.

Acknowledgments: We thank A/Prof Michelle Monje, Dr Angel Montero Carcaboso and Dr Esther Hulleman for generously supplying the SU-DIPG, HSJD-DIPG and VUMC-DIPG10 cells, respectively and the Core Services Group at Children's Cancer Institute for their technical support. We thank Dr Barry Maurer for generously supplying the Fenretinide LYM-X-SORB formulation. Mass spectrometric results were obtained at the Bioanalytical Mass Spectrometry Facility within the Mark Wainwright Analytical Centre of the University of New South Wales. We thank the Biological Resources Imaging Laboratory (BRIL) at the University of New South Wales for technical assistance. RNA sequencing was performed at the Ramaciotti Centre for Genomics at the University of New South Wales, Sydney, Australia.

Funding:

National Health and Medical Research Council, (DSZ, AK) Synergy Grant #2019056

National Health and Medical Research Council, Investigator Grant APP2017898, (DSZ)

Cancer Institute New South Wales Program Grant (TPG2037), (DSZ)

Cancer Australia, Cancer Council NSW, (DSZ)

Cure Brain Cancer Foundation, (DSZ, MT)

The DIPG Collaborative, The Cure Starts Now, (MT, DSZ)

Levi's Project, (MT, DSZ)

Benny Wills Foundation, (DSZ)

Author contributions:

Conceptualization: DU, MT. DSZ

Methodology: IO, GF, PR

Investigation: DU, JL, SG, SV, NY, CU, BR, AG, RP, AK, LF, AE, PV, CM, MT

Funding acquisition: MT, DSZ

Supervision: MT, DSZ

Writing - original draft: DU

Writing - review & editing: DU, MT, DSZ

Competing interests: DSZ reports consulting / advisory board fees from Bayer, Astra Zeneca, Accendatech, Novartis, Day One, FivePhusion, Amgen, Alexion, and Norgine and research support from Accendatech.

Data materials availability: All data are available in the main text or the supplementary materials

Figure Legends

Figure 1. High-throughput screening and identification of new compounds with anti-DMG activities. Primary screening results of 3,570 compounds against DMG, which were arranged in order of percentage cell viability. Red data points indicate the top 90 hits identified through HTS. **(A)** SU-DIPGVI cells treated with 10 µM of each compound and **(B)** HSJD-DIPG007 cells treated with 5 µM of each compound. Drug cytotoxicity was assessed in SU-DIPGVI, HSJD-DIPG007 and MRC5 cells. All drugs examined showed a dose-dependent cell viability reduction (**C**) Lanatoside C (**D**) Ivermectin (**E**) Fenretinide (**F**) SAHA (**G**) Mefloquine hydrochloride (**H**) Parthenolide. (N=3) **= $p<0.005$*** = $p<0.001$.

Figure 2. Fenretinide increases survival in an in vivo HSJD-DIPG007 orthotopic model. Kaplan-Meier plot of percentage survival of HSJD-DIPG007-xenografted BalbC/Nude mice treated with **(A)** lanatoside C **(B)** ivermectin **(C)** LYM-X-SORB fenretinide. (**D**) Quantification of Ki67 staining following treatment with LYM-X-SORB fenretinide, * = $p<0.05$. (**E**) Pharmacokinetic analysis following fenretinide treatment. Kaplan-Meier plot of percentage survival of HSJD-DIPG007-xenografted BalbC/Nude mice treated with **(F)** SAHA **(G)** mefloquine hydrochloride **(H)** parthenolide.

Figure 3. Fenretinide induces the production of reactive oxygen species (ROS), apoptosis and affects PDGFRα in DMG. (A) ROS production in HSJD-DIPG007 fenretinide treated cells over time (30 minutes to 4 hours). Antimycin was used as a positive control. *** = $p<0.001$. (N=3) **(B)** Luminescence quantification of induction of caspase 3/7, in HSJD-DIPG007 cells treated with fenretinide. (N=2) **(C)** Western blot of HSJD-DIPG007 treated

with fenretinide for 24 and 48 hours. (N=3) **(D)** Quantification of apoptosis in HSJD-DIPG007 cells treated with fenretinide. Columns represent apoptotic events at 24 hours at different concentrations of fenretinide (mean ±SEM). * = p<0.05, ***=p<0.001. (N=2**(E)** Western blot of HSJD-DIPG007 treated with fenretinide for 24 and 48 hours. (N=3) **((F)** Expression of PDGFRα mRNA as quantified by real-time PCR in HSJD-DIPG007 cells treated with fenretinide for 24 or 48 hours. Expression levels of PDGFRα were normalized to the GAPDH control, and expression was compared between the untreated and treated samples. (N=2) **(G)** Western blot of HSJD-DIPG007 treated with fenretinide for 24 and 48 hours. (N=3) **(H)** Western blot of RA055 cells treated with fenretinide for 24 and 48 hours. (N=3) **(I)** Western blot of RA055 cells treated with fenretinide for 24 and 48 hours. (N=3) **(J)** Western blot of RA055 cells treated with fenretinide for 24 and 48 hours. (N=3)

Figure 4. Fenretinide treatment upregulates ER stress and unfolded protein response in DMG cells. (A) Top 20 upregulated gene ontology (biological processes) identified through RNA sequencing analysis in HSJD-DIPG007 cells treated with 2 µM fenretinide for 24 hours Expression of **(B)** Atf4, **(C)** Chop, **(D)** Bip and **(E)** sXbp1 mRNA as quantified by real-time PCR in HSJD-DIPG007 and RA055 cells treated with fenretinide for 24 hours. Gene expression levels were normalized to the 18s/B2m control, and expression was compared between the untreated and treated samples. * = p<0.05, **=p<0.005.

Figure 5. Fenretinide treatment down regulates markers of neural stem cells in DMG cells. (A) Top downregulated gene ontology (biological processes) identified through RNA sequencing analysis in HSJD-DIPG007 cells treated with 2 µM fenretinide for 24 hours Expression of **(B)** Ascl1, **(C)** Cl-Notch1 **(D)** Notch1 **(E)** Hes1 **(F)** Lef1, **(G)** Nestin, **(H)** Olig2,

(I) Dll1 mRNA as quantified by real-time PCR in HSJD-DIPG007 and RA055 cells treated with fenretinide for 24 hours. Gene expression levels were normalized to the 18s/B2M control, and expression was compared between the untreated and treated samples. * = $p<0.05$, **=$p<0.005$.

Figure 6. Fenretinide is active against PDGFRα-amplified DMG models (A) Kaplan-Meier plot of percentage survival of PDGFRa-amplified DMG -xenografted BalbC/Nude mice treated with LYM-X-SORB fenretinide or vehicle control. **(B)** Kaplan-Meier plot of percentage survival of PDGFRa-amplified DMG -xenografted BalbC/Nude mice treated with nanomicellar fenretinide or nanomicelles. **(C)** Kaplan-Meier plot of percentage survival of murine DMG cells (H3.3/K27M, TP53loss, PDGFRA/D842V) engrafted in C57/BL6 animals treated with LYM-X-SORB fenretinide or vehicle. **(D)** Pharmacokinetic analysis performed in the brains of animals post-treatment with fenretinide. **(E)** Representative Ki67 staining images and resulting quantification of DMG tumours post LYM-X-SORB fenretinide treatment. **(F)** Representative Ki67 staining images and resulting quantification of DMG tumours post nanomicellar fenretinide treatment. **(G)** Representative PDGFRα staining images and resulting quantification of DMG tumours post LYM-X-SORB fenretinide treatment. **(H)** Representative PDGFRα staining images and resulting quantification of DMG tumours post nanomicellar fenretinide treatment. The black scale bar on each image indicates 50 µm.

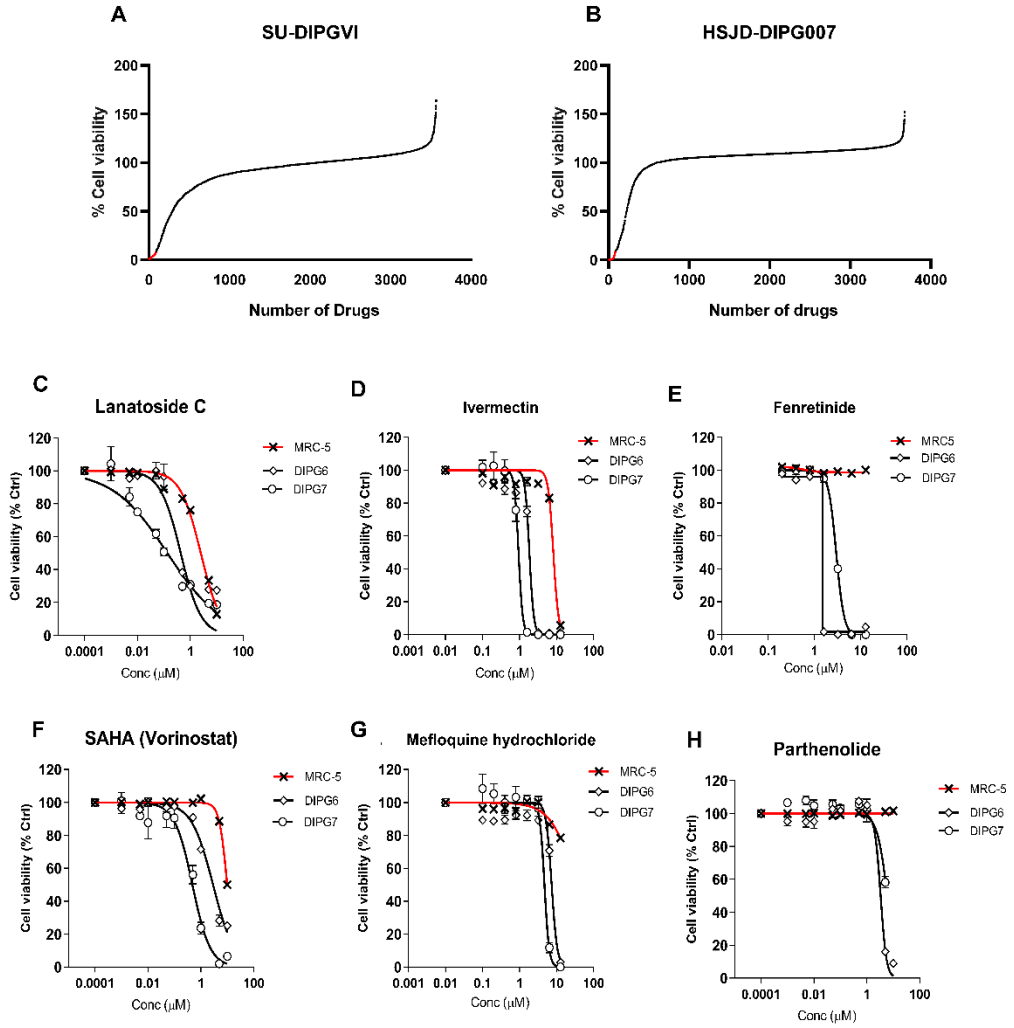

Figure 1

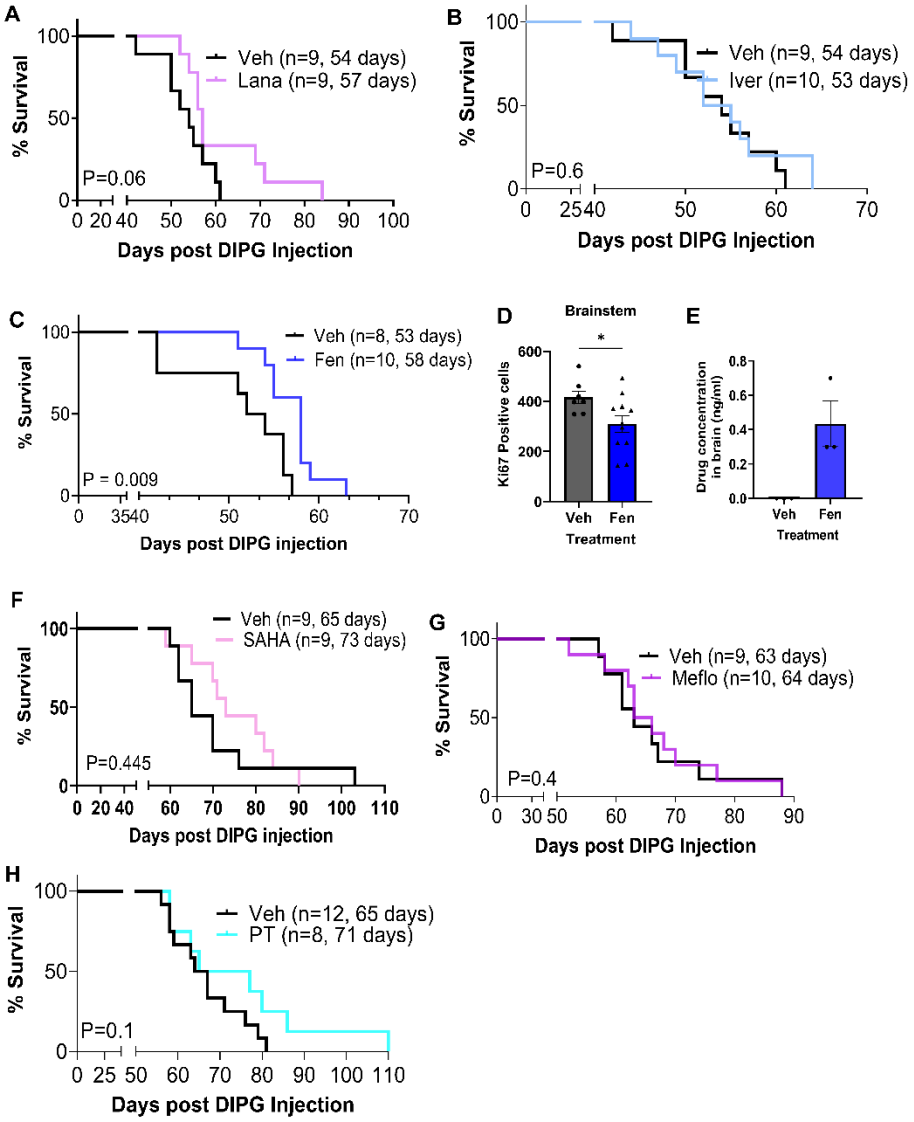

Figure 2

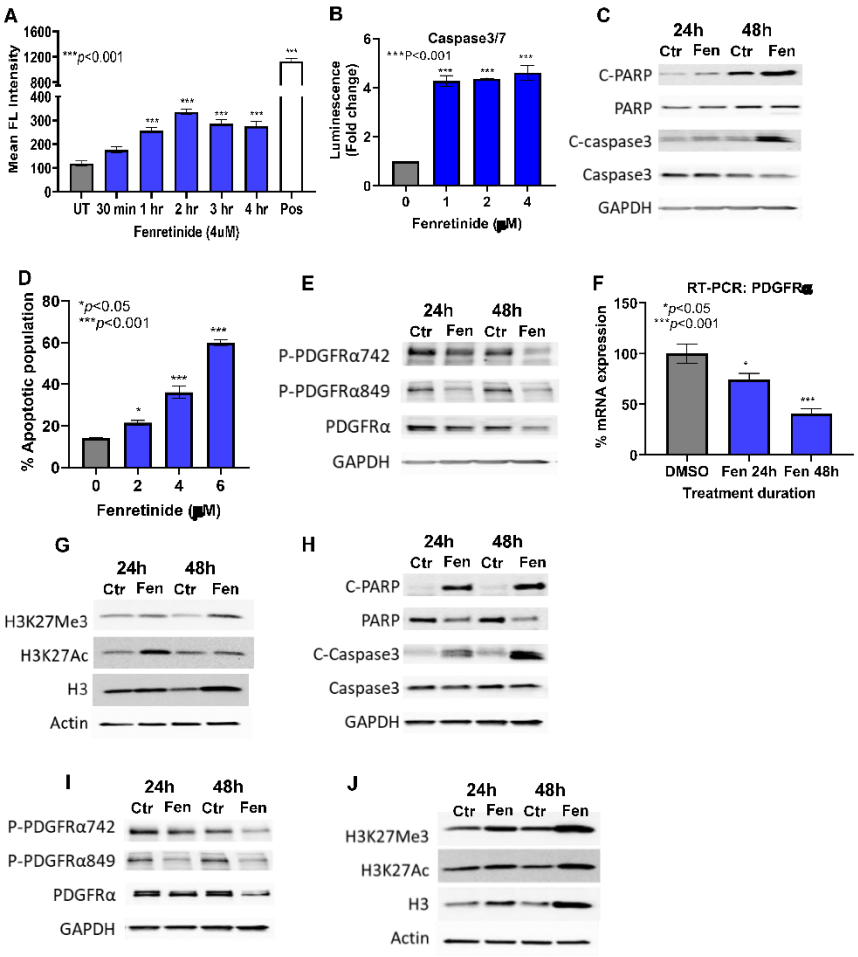

Figure 3

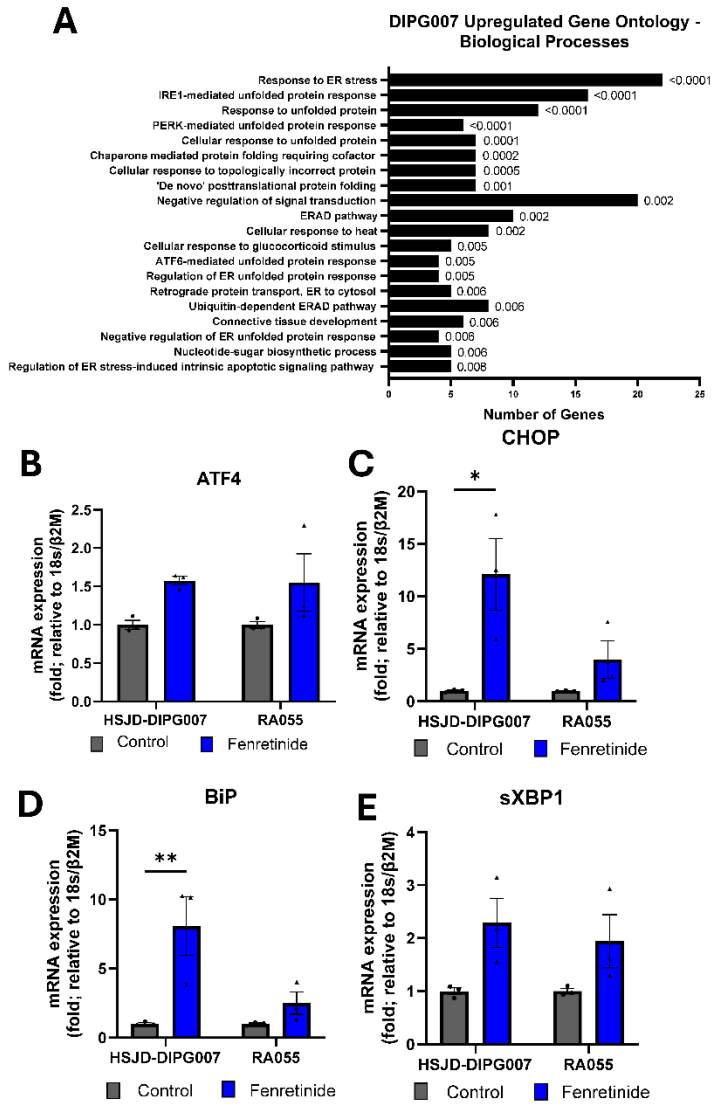

Figure 4

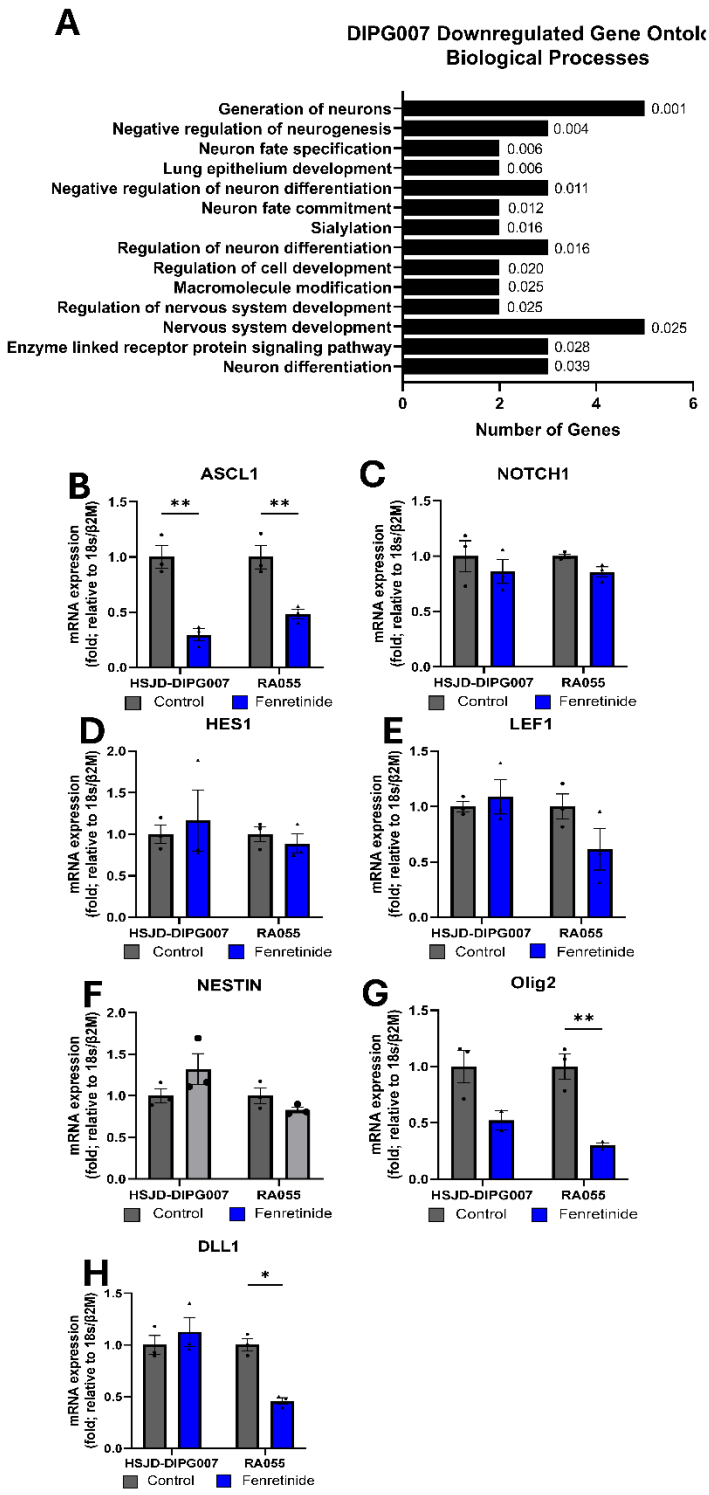

Figure 5

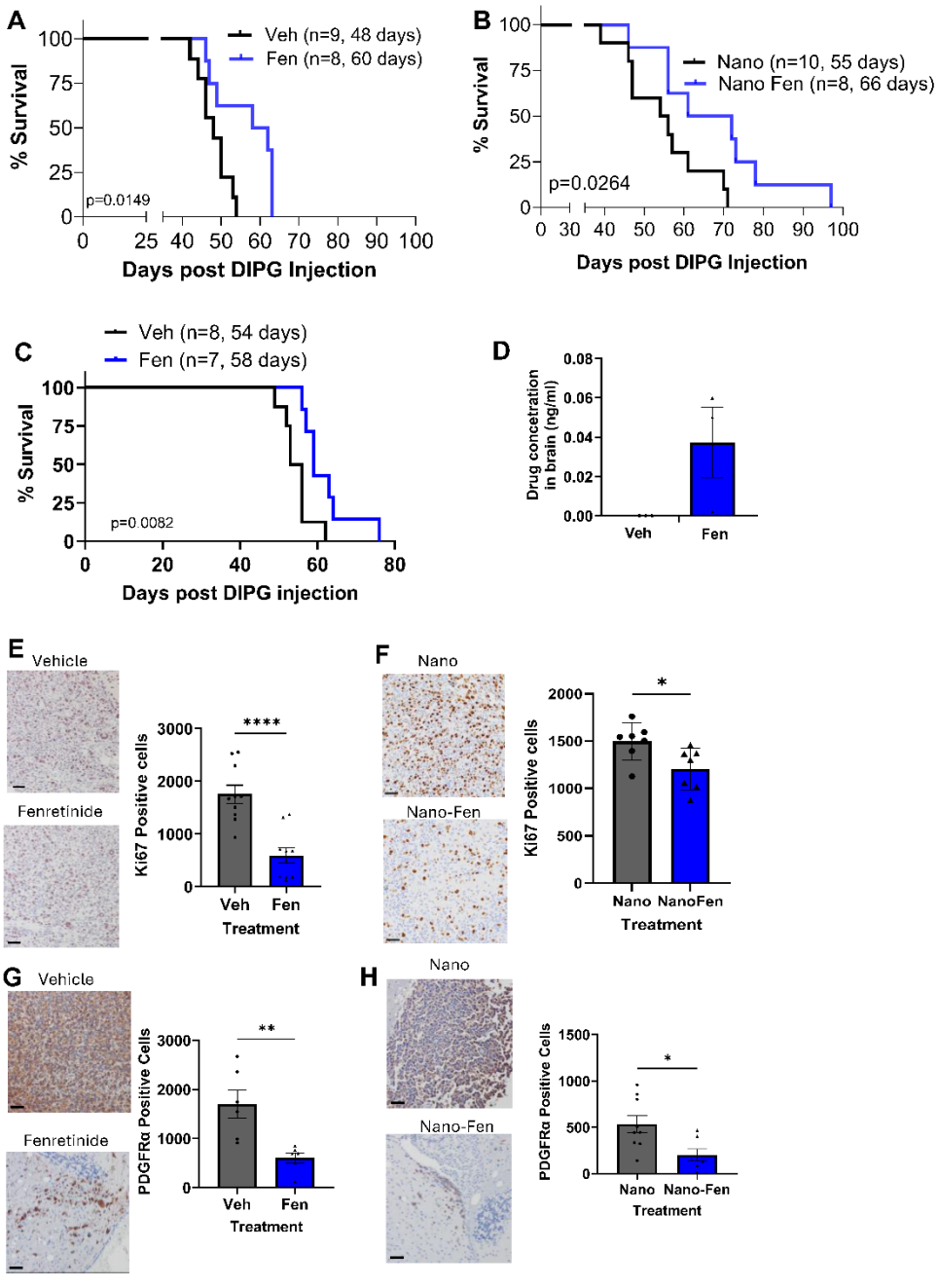

Figure 6